Exploring control landscapes for laser-driven molecular fragmentation

Cite as: J. Chem. Phys. **139**, 144201 (2013); https://doi.org/10.1063/1.4824153
Submitted: 14 June 2013 . Accepted: 20 September 2013 . Published Online: 08 October 2013

Katharine Moore Tibbetts, Xi Xing, and Herschel Rabitz

Exploring control landscapes for laser-driven molecular fragmentation

Katharine Moore Tibbetts,[a] Xi Xing, and Herschel Rabitz
Department of Chemistry, Princeton University, Princeton, New Jersey 08544, USA

(Received 14 June 2013; accepted 20 September 2013; published online 8 October 2013)

The growing success of quantum optimal control experiments has been attributed to the favorable topology of the *control landscape*, which specifies the functional relationship between the physical objective and the control variables describing the applied field. This work explores experimental control landscapes expressing the yields of dissociative ionization products from halogenated hydrocarbons in terms of three control variables specifying a polynomial expansion of the spectral phase of the ultrafast laser pulse. Many of the landscapes in this work exhibit features predicted by control landscape theory, including a lack of suboptimal extrema, i.e., "traps" and the presence of connected optimal level sets, i.e., continuously varying values of the control variables that produce an optimal objective yield. Placing significant constraints on the control resources, particularly by limiting the laser pulse energy, was found to distort the underlying landscape topology. The control landscapes from a diverse, yet related family of halogenated hydrocarbons are shown to possess similar features, reflecting the chemical similarity of the compounds. © *2013 AIP Publishing LLC*. [http://dx.doi.org/10.1063/1.4824153]

I. INTRODUCTION

Optimal control of quantum systems with applied fields is enjoying growing experimental success. Closed-loop optimal control experiments (OCE)[1] with ultrafast shaped laser pulses have successfully manipulated many physical and chemical objectives including excited state preparation,[2,3] generation of high-order harmonics,[4–6] energy transfer and isomerization in biomolecules,[7–9] and molecular dissociation,[10–18] with over 100 successful studies reported in the literature.[19] Numerical simulations using optimal control theory (OCT)[20] to search for a control field also routinely achieve nearly 100% of the theoretical yield for many different objectives.[19]

The broad success of optimally controlling the dynamics of quantum systems is attributed to the favorable topology of the underlying *control landscape*, which specifies the functional relationship between the physical objective and the applied field. The physical objective $J[\varepsilon(t)]$ is expressed as the expectation value of a quantum observable at a target time T, $0 \le t \le T$,

$$J[\varepsilon(t)] \equiv \mathrm{Tr}(\rho[\varepsilon(t)]\Theta). \tag{1}$$

Here, $\rho[\epsilon(t)]$ is the density matrix at time T describing the state of the quantum system after interaction with the field $\varepsilon(t)$, $0 \le t \le T$, and Θ is a Hermitian observable operator describing the target objective. Theoretical analysis[21–24] shows that quantum control landscapes $J[\varepsilon(t)]$ of closed systems contain no suboptimal extrema, or "traps," that prevent the attainment of the globally optimal objective yield, upon satisfaction of the following physical Assumptions:

(i) The target system is *controllable*, i.e., some choice of the field $\varepsilon(t)$, $0 \le t \le T$, exists that maximizes the target objective.[25]

(ii) The map from the space of fields $\varepsilon(t)$ to the associated dynamical propagators $\rho[\varepsilon(t)]$ is surjective,[26,27] such that a small arbitrary variation of the state ρ at time T has an associated small variation in $\varepsilon(t)$, $0 \le t \le T$.

(iii) No constraints are placed on the control field $\epsilon(t)$, so that free movement over the control landscape is permitted.

When the latter Assumptions are satisfied for objective functionals of the form in Eq. (1), the trap-free topology of the control landscape follows from mathematical analysis.[21–24]

Satisfaction of the Assumptions is *sufficient* for establishing the control landscape topology, and a practical issue is the degree to which the very attractive landscape conclusions still apply even when the Assumptions are not fully satisfied. The present experiments under commonly attainable laboratory conditions for laser-induced dissociative ionization represent a good testing ground for this matter. Although Assumption (i) can be violated, it is likely to be satisfied to a practical degree for most quantum systems.[28] In particular, the ability to simply reach the target state may be adequate, rather than the nominal demand of full state controllability in Assumption (i). Assumption (ii) has the unusual property that its likelihood of being satisfied should generally increase with system complexity, which enhances the freedom to locally transform the state.[26,27,29] In contrast, Assumption (iii) can easily be violated in the laboratory because the control pulse energy, center wavelength, spectral bandwidth, etc., are inherently limited. Thus, it is of particular interest to experimentally explore quantum control landscapes in order to assess the degree to which limited resources impede the search for optimal control fields by permitting access to only a restricted portion of the underlying favorable landscape topology.

Analyses of the control landscape topology and the associated Assumptions have been performed in the context of a finite dimensional quantum system,[22,23,26,27] while many

[a]Present address: Department of Chemistry, Temple University, Philadelphia, Pennsylvania 19122, USA.

experiments, particularly for molecular fragmentation, nominally go beyond having a finite number of states. In addition, most numerical simulations of the topology and local structure of quantum control landscapes have been conducted with model finite-dimensional systems that also remove constraints on $\varepsilon(t)$ to the extent possible.[30–33] These investigations have confirmed the predicted lack of traps on the control landscape when no significant constraints are placed on the control field, while further numerical simulations have found that imposing significant constraints on the control variables can cause traps to arise on the control landscape,[34] that can limit the maximum attainable objective yield.[35,36]

Control landscape theory also predicts the existence of connected optimal level sets on the landscape, which consist of families of controls that may be continuously morphed from one to another, while maintaining an optimal objective yield.[22,23] Additionally, the theory does not preclude the existence of multiple disconnected level sets. Numerical simulations exploring optimal level sets (i.e., at the maximum yield) have revealed diverse families of fields that transfer population to a selected excited state.[33,34] Placing significant constraints on the control field has been shown in numerical simulations to fracture optimal level sets into disconnected regions, where the level sets ultimately shrink to points and then pull away from the top of the landscape as further constraints are imposed.[34] Connected level sets of fields producing suboptimal objective yields have also been explored in numerical simulations[37] and experiments for second harmonic generation and non-resonant two-photon absorption.[38]

As some laboratory constraints on the field $\varepsilon(t)$ are inevitable, which can possibly violate Assumption (iii), the experimental exploration of landscapes is of particular interest to gauge the potential for effective optimization. At the same time, it is often desirable to operate experiments with reduced control bases to simplify interpretation of the control processes,[39] which allows for direct landscape visualization with two or three control variables. Experimental control landscapes expressed in terms of two or three control variables have been presented for a variety of target objectives, including second harmonic generation (SHG),[38,40] non-resonant two-photon absorption (TPA) in a laser dye,[38] spectrally filtered SHG,[40] third harmonic generation (THG) and stimulated emission in a laser dye,[41] three-photon absorption in I_2,[42] population transfer in porphyrazines[43] and a laser dye,[44] and photoisomerization in bacteriorhodopsin.[45] The latter objectives are in the form of Eq. (1), and the lack of traps (to within reasonable experimental noise) observed on the associated landscapes[38,40–45] indicates that in these cases, the limited number and type of control variables describing $\varepsilon(t)$ appear sufficient to satisfy Assumption (iii). A trap recorded on the THG landscape in Ref. 41 was attributed to imperfections in the phase-matching angles in their experimental setup, indicating the presence of constraints on the control variables. Simulated control landscapes for SHG and coherent anti-Stokes Raman spectroscopy (CARS) were also found to have a trap-free topology upon utilizing a suitable choice of control variables.[46,47] When the objective is not in the form of Eq. (1), the present formulation of control landscape theory cannot make a general assessment of the resulting landscape topology. A common example is when the objective is expressed as the ratio of two experimental observations, as a ratio is not the expectation value of a Hermitian operator. In this regard, traps have been found on experimental control landscapes for objectives defined by ratios of excited state populations[48,49] and fragmentation products of molecular dissociation.[13,18]

This work will explore control landscapes for selective fragmentation objectives in the halogenated hydrocarbons CH_2BrCl, CH_2Br_2, CH_2IBr, CH_2I_2, C_3H_5Br (mixture of *cis/trans* 1-bromo-1-propene), C_4H_7Cl (3-chloro-2methyl-1-propene), and C_6H_5Cl (chlorobenzene), with an emphasis on CH_2IBr as an illustrative case. Although optimal control of molecular fragmentation commonly employs ratios of product yields to define the objective,[10–18] observables of the form in Eq. (1) will be considered exclusively in this work so that the predictions of control landscape theory may be assessed. Specifically, control landscapes will be constructed for the two ionized photoproducts R^+ and X^+ resulting from cleavage of one carbon-halogen bond in molecules R−X, where R denotes the hydrocarbon-based fragment and X denotes the halogen. The three control variables utilized here describe a polynomial expansion of the spectral phase $\Phi(\omega)$ of the laser pulse: $\Phi(\omega) = A(\omega - \omega_0)^2 + B(\omega - \omega_0)^3 + C(\omega - \omega_0)^4$. These control variables A, B, and C were found to enable extensive manipulation of the relative yields of R^+ and X^+ in a family of 11 halomethanes,[17,18,50] and have been shown to effectively control population transfer in a pair of porphyrazines.[43] The polynomial phase functions $(\omega - \omega_0)^n$, $n = 2, 3, 4$ are flexible and linearly independent, but truncation of the polynomial phase expansion to low order produces constrained fields that provide a stringent test of the control landscape theory predictions. We will also explore how reducing the number of polynomial functions, as well as the laser pulse energy, impacts the landscape features. These tests also assess control landscape theory beyond its rigorous formulation by considering dissociative processes that involve a continuum of states (i.e., beyond finite-dimensional quantum systems).

The family of chemically homologous substrates listed above is chosen to determine the degree to which the respective control landscapes exhibit common features due to the chemical similarity of the substrates. Related families of shaped ultrafast laser pulses have been found to produce systematic correlations between the relative yields of photoproducts and the substrate's halogen composition over a large family of halomethanes.[17,50] The latter results provide a basis to consider shaped ultrafast laser pulses as "photonic reagents" in analogy with the systematic behavior commonly found with the reactions induced by chemical reagents over a family of related substrates. Recently, so-called OptiChem theory[51,52] was introduced, which predicts the existence of the same control landscape features (i.e., no traps and the possible presence of optimal level sets) upon satisfaction of Assumptions (i)–(iii) when the control variables describe chemical reagents instead of photonic reagents. The present work will further cement the connections between these two optimal control paradigms by investigating the features of control landscapes for photonic reagent control of chemical substrates

that form a homologous family of molecules under traditional chemical notions. In particular, we seek photonic reagent and substrate "rules" for predicting the general features of landscapes for R^+ and X^+ yields, in analogy to such commonly employed empirical rules in chemistry for predicting the outcomes of reactions between chemical reagents and substrates.

The remainder of the paper is structured as follows. Section II describes the experimental apparatus and the methods used for landscape visualization. Section III explores control landscapes for CH_2IBr, including optimal level sets as well as the effects of further constraining the polynomial control variables and laser pulse energy. Section IV presents control landscapes for the remaining halogenated hydrocarbons. Section V examines the shared features of the control landscapes across the substrate family to formulate rules for predicting the structure of control landscapes for the fragmentation products R^+ and X^+. Section VI assesses the extent to which landscape theory predictions are satisfied with a low-order polynomial phase representation of the control field and discusses the physical consequences. Finally, Sec. VII presents concluding remarks.

II. EXPERIMENTAL METHODS

The experiments employed a Ti:Sapphire oscillator and amplifier (KM Labs, Inc.) generating 1.9 mJ pulses centered at 791 nm with a gain-flattening filter (ARO, SF640) to produce a bandwidth FWHM of 50 nm and pulse duration of ∼25 fs. The laser pulses were shaped with a programmable dual-mask liquid crystal spatial light modulator (SLM) with 640 pixels and 0.179 nm/pixel resolution (CRI, SLM-640) capable of independent phase and amplitude modulation. The output pulse energy from the shaper was approximately 350μJ. Phase-amplitude coupling in the SLM was sufficiently small such that the pulse energy could be varied by amplitude shaping without changing the spectral phase (i.e., verified by two-photon absorption). Similarly, placing arbitrary spectral phases on the SLM only decreased the output pulse energy to ∼345 μJ. To remove residual high-order dispersion from the amplifier output, the SLM phase corresponding to the transform-limited (TL) pulse was identified with a genetic algorithm (GA) by optimizing the two-photon absorption (TPA) signal measured by a two-photon diode (Thorlabs) and a boxcar integrator; this reference phase was added to all subsequent phases placed on the SLM.

The shaped pulses were focused with a fused silica lens of $f = 20$ cm into a vacuum chamber, producing a knife-edge measured spot size of 45 μm with an estimated maximum peak intensity of $\sim 8 \times 10^{14}$ W/cm^2. A linear time-of-flight (TOF) mass spectrometer was used to detect the products of the laser-induced fragmentation with the laser radiation polarized parallel to the TOF axis. The molecular samples were purchased from Sigma-Aldrich and used without further purification. The samples were introduced into the vacuum chamber (base pressure 1.0×10^{-8} Torr) through an effusive leak valve to maintain a pressure of 1.0×10^{-6} Torr during the experiments. The ion extraction plate had a pinhole 0.5 mm in diameter to ensure collection of ions only from the laser focal region, as well as to reduce the effects of spatio-temporal coupling of the focused laser beam that can produce different temporal fields across the focal region.[53,54] Any residual spatio-temporal effects were normalized over the set of molecules by using the same apparatus. The ions passed through a grounded plate into a 1 m field-free flight tube to an 18 mm dual microchannel-plate detector (Jordan, C-701). The resulting TOF spectra were recorded with a digital oscilloscope (LeCroy 104MXi) and averaged over 20 000 laser shots.

The experiments employed compounds of the form R−X, with R being a hydrocarbon-based moiety and X being a halogen atom. We consider the dissociative ionization of R−X to form R^+ or X^+, where the control landscapes for the respective ion yields are examined:

- **R^+ yield:** CH_2Cl^+ (from CH_2BrCl), CH_2Br^+ (from CH_2IBr, CH_2BrCl, and CH_2Br_2), CH_2I^+ (from CH_2IBr and CH_2I_2), $C_3H_5^+$ (from C_3H_5Br), $C_4H_7^+$ (from C_4H_7Cl), and $C_6H_5^+$ (from C_6H_5Cl).
- **X^+ yield:** Cl^+ (from CH_2BrCl, C_4H_7Cl, and C_6H_5Cl), Br^+ (from CH_2BrCl, CH_2Br_2, CH_2IBr, and C_3H_5Br), and I^+ (from CH_2IBr and CH_2I_2).

The yield of each product is measured by integrating over the full width of the corresponding ion signal in the TOF spectrum. This definition of the objective yield satisfies the form in Eq. (1), thereby permitting the predictions of control landscape theory to be assessed. In some cases, landscapes are generated for products that correspond to, respectively, breaking either the strong or weak carbon-halogen bonds (e.g., CH_2I^+ and CH_2Br^+ from CH_2IBr). Each case forms a unique landscape for physical analysis, regardless of the commonly sought after goal of breaking the strong bond over the weak bond.

Control landscapes for the yield of each fragmentation product constructed with respect to three control variables allow for direct visualization of the landscapes; the laser pulse energy will form an additional variable for investigation in Sec. III C. The control variables A, B, and C define a polynomial spectral phase $\Phi(\omega)$ as a function of the frequency ω:

$$\Phi(\omega) = A(\omega - \omega_0)^2 + B(\omega - \omega_0)^3 + C(\omega - \omega_0)^4, \quad (2)$$

where ω_0 denotes the center spectral frequency of the laser radiation. A polynomial spectral phase is equivalent to a truncated Taylor expansion of the spectral phase around the center frequency ω_0,

$$\Phi(\omega) = \Phi(\omega_0) + \Phi'(\omega)(\omega - \omega_0) + \frac{1}{2}\Phi''(\omega)(\omega - \omega_0)^2 + \frac{1}{6}\Phi'''(\omega)(\omega - \omega_0)^3 + \frac{1}{12}\Phi''''(\omega)(\omega - \omega_0)^4 + \ldots. \quad (3)$$

The zeroth- and first-order terms in Eq. (3) do not contribute to the temporal shape of the laser pulse, while the control variables A, B, and C in Eq. (2) represent the second-, third-, and fourth-order terms of the Taylor expansion, respectively. Their values are varied over the ranges $A = \pm 2 \times 10^4$ fs^2, $B = \pm 4 \times 10^5$fs^3, and $C = \pm 8 \times 10^6$ fs^4, which are within the

resolution limits of the SLM. The value of each control variable was scanned in 9 steps over its range to produce a total of $9^3 = 729$ pulse shapes corresponding to distinct points on the three-dimensional control landscape. The integrated yield of each target ion from the resultant 729 TOF spectra was measured for the construction of the landscapes. All objective yields on the landscape are reported as the fractional yield of the integrated ion signal relative to the maximum recorded yield across the 729 values, where 95% of the maximum yield of each objective is considered optimal to within experimental noise throughout this work. For reference, closed-loop optimization of the ratio Br^+/CH_2Br^+ in CH_2IBr using the methods in Ref. 17 with additional higher order terms in the Taylor expansion of Eq. (3) did not improve the maximum ratio yield beyond that recorded with the three control variables in Eq. (2) (not shown), so we expect that the most significant features of the landscapes can be accessed with only the three control variable specifying up to the fourth order term in Eq. (3). Although we cannot assure that the absolute top of the landscape is reached upon optimization with the variables in Eq. (2), experiments optimizing a ratio X^+/R^+ produced yields $\gtrsim$25 relative to the TL pulse, indicating that the polynomial control variables provide considerable freedom for this application. Thus, we will refer to the landscapes as unconstrained upon free variation of A, B, and C while employing the maximum available pulse energy. Furthermore, landscape visualization becomes impossible with additional variables, so the present three control variables are a good practical choice for assessing the present landscapes. The degree to which the control landscape Assumptions and principles summarized in Sec. I are satisfied will attest to the adequacy of these variables.

The landscapes may be visualized by plotting the level set surfaces corresponding to fractional objective yields of 95% through 5% as a function of A, B, and C, with the color of the level set surface denoting the fractional objective yield. To construct these level set surfaces, spline interpolation between the experimental landscape points was performed to estimate the corresponding objective yield for graphical presentation. These surfaces are plotted using the `isosurface` function in MATLAB.[55] All major landscape features (i.e., the location and size of local and global maxima and minima) were reproducible with mass spectral data from the same molecule measured on different occasions in the laboratory.

We first present the landscape of TPA yield measured by the two-photon diode as a function of A, B, and C, to illustrate landscape visualization as well as to provide a reference for the photoproduct landscapes presented later. The two views of the landscapes that will be presented in this work are shown for the TPA landscape in Figure 1. The view (a) shows the level sets at 20% and 40% yield over the full volume, where the optimal landscape point at the TL pulse with $A = B = C = 0$ is obscured because it lies *inside* the level set corresponding to 40% yield. In order to visualize the optimal region, the second perspective splits the landscape down the dashed line (corresponding to $A = 0$) in Figure 1(a), producing the landscape view (b). Landscapes for fragmentation product yields will be shown with the suitable view that allows the clearest visualization of the optimal landscape regions.

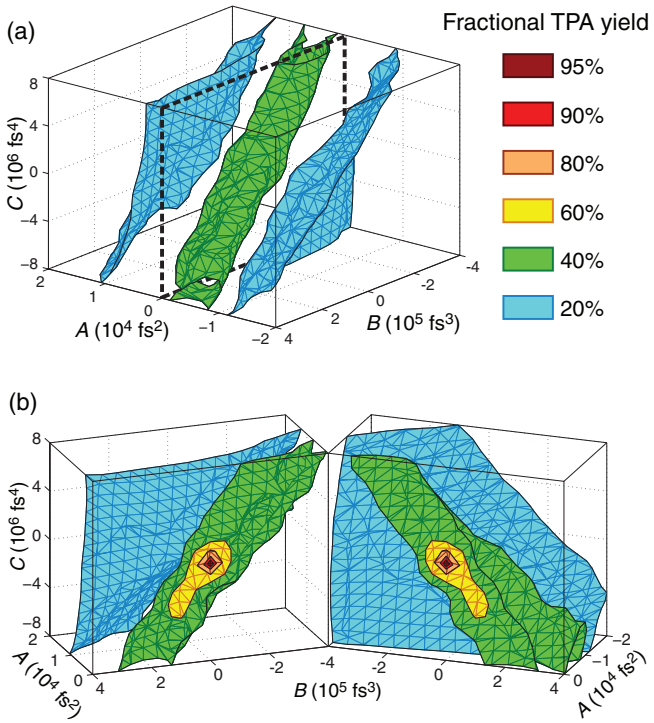

FIG. 1. Control landscape for TPA yield showing the fractional yields: 95% (maroon), 90% (red), 80% (orange), 60% (yellow), 40% (green), and 20% (cyan). (a) View of the landscape as a single total volume, with only the level sets corresponding to 40% and 20% yield visible and the level sets corresponding to 60% yield and above obscured. (b) Split view of the landscape along $A = 0$, corresponding to the dashed line in (a), which permits visualization of the optimal landscape region at the TL pulse with $A = B = C = 0$.

Examination of the TPA landscape prior to investigating the photoproduct landscapes is important because it provides insight into the behavior of an intensity-driven process, as well as possibly revealing any limitations of the experimental apparatus. The level sets near the top ($\gtrsim$90% relative yield) of the non-resonant TPA landscape have been analytically shown to have the form of an off-axis ellipsoid in the polynomial spectral phase basis, and level sets at lower yield were experimentally observed to exhibit inversion symmetry through $A = B = C = 0$.[38] These ellipsoidal features are evident for the level sets in Figure 1. However, the 60% (yellow) level set in Figure 1(b) extends farther into the region of $C < 0$ than into the region of $C > 0$, thus breaking the inversion symmetry. This deviation is substantially away from the maximum yield domain where the behavior is well understood, but it may possibly arise from an artifact of resolution limitations in the SLM. Imperfections in the optical alignment anywhere in our experimental set-up may contribute to this distortion as well. The higher TPA signal at $C < 0$ is reflected in increased ion yields in this region for some of the landscapes presented below, which is consistent with intensity being a main control factor for absolute ion yields in these cases; these situations are noted in the following discussion. Finally, we note that the TPA signal is measured before the focusing lens, so a small amount of dispersion is uncompensated in the TOF chamber. However, this dispersion is expected to be insignificant compared to the variation of A, B, and C explored.

III. CONTROL LANDSCAPES FOR BROMOIODOMETHANE

The most detailed investigations in this work are conducted with CH_2IBr as an illustration of the features of control landscapes for photofragmentation products. Section III A investigates the features of unconstrained landscapes using the maximum available pulse energy and all three variables A, B, and C. The optimal level set regions of the landscape for Br^+ are explored in Sec. III B, while Sec. III C investigates the effects of placing constraints on these control variables.

A. Topology of unconstrained landscapes

Control landscapes are shown in Figure 2 for the objective yields of (a) CH_2Br^+, (b) Br^+, (c) CH_2I^+, and (d) I^+. In order to visualize the regions of maximum objective yield, the landscapes (a) and (c) are shown split, as in Figure 1(b). These landscapes for CH_2Br^+ and CH_2I^+ are of similar structure to the TPA landscape in Figure 1(b), with the landscape maximum at the TL pulse $A = B = C = 0$ and the orientation of the fractional yield level sets along the same axis as the level sets on the TPA landscape. This similarity between the R^+ and TPA landscapes implies that the yields of the R^+ ions are primarily dependent on the laser intensity. A second maximum occurs at a slightly positive value of B and negative value of C on both R^+ landscapes. It is difficult to tell if it is an isolated second maximum consistent with the higher TPA signal at $C < 0$ (cf., Figure 1(b)) or just a broad maximum beyond any of the many small measurement artifacts estimated to produce errors at the ∼5% level. In contrast, the landscapes for Br^+ and I^+ in (b) and (d), respectively, exhibit distinct structures far away from the TL pulse, with two disconnected regions producing an optimal objective yield. The existence of two disconnected landscape maxima away from the TL pulse indicates that the Br^+ and I^+ yields are only weakly dependent on the laser intensity. This feature is consistent with the results in Ref. 50 where the maximum halogen ion yield upon variation of A in Eq. (2) was found to occur at distinct nonzero values of A. Within the limits of resolution, the landscapes in Figure 2 do not exhibit trapping regions, indicating that the Assumptions of control landscape theory appear to be satisfied, especially that the three control variables are sufficient to satisfy Assumption (iii) for producing R^+ and X^+ from the fragmentation of CH_2IBr. All of the landscapes in Figure 2 (as well as the landscapes for other molecules presented in Sec. IV) display some asymmetry with respect to the sign of A, while the TPA landscape is nearly symmetric with respect to the sign of A. This asymmetry likely arises from differences in the photophysics under positively and negatively chirped pulses; similar chirp effects have been observed in several classes of molecules.[50,56–58]

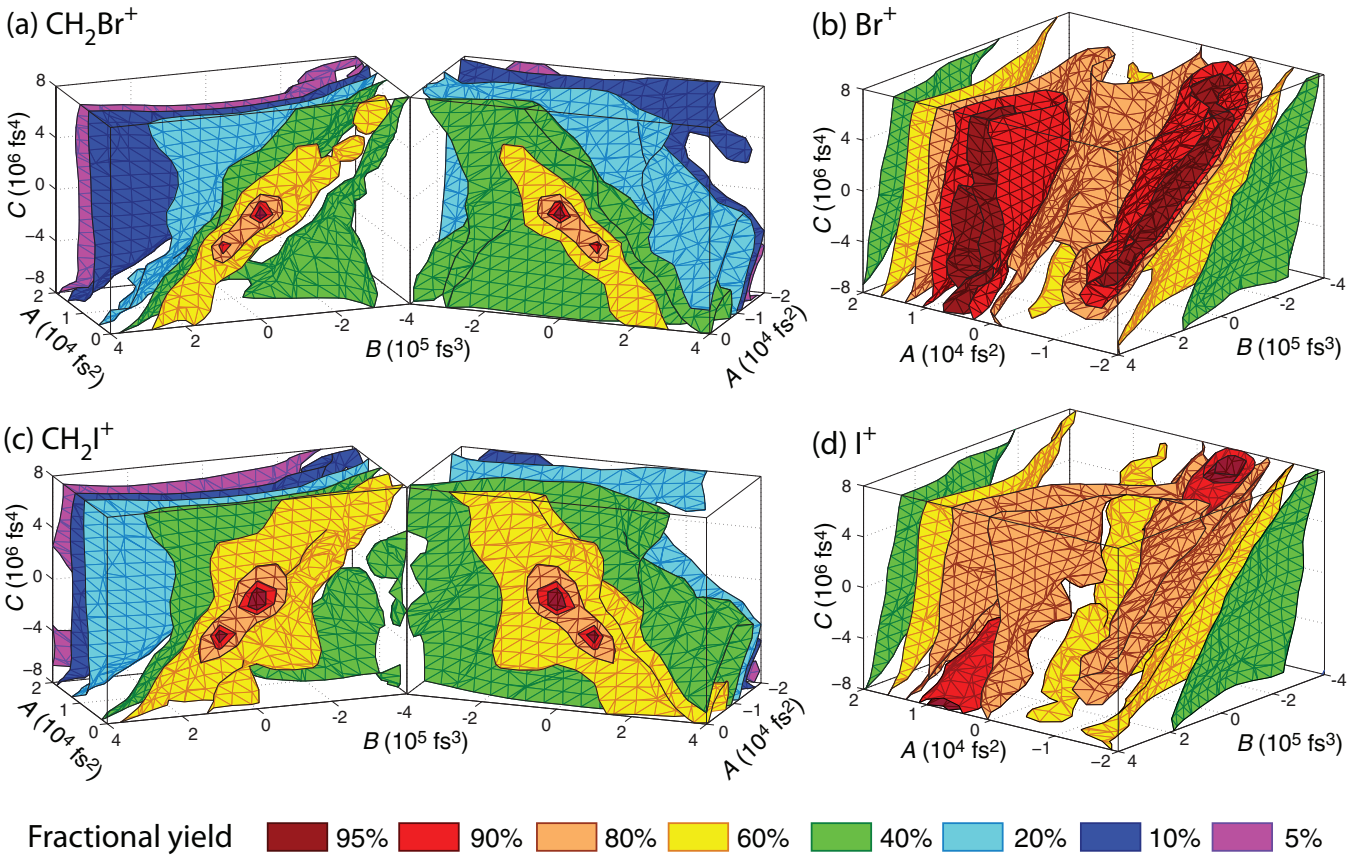

FIG. 2. Control landscapes for ionized fragmentation products of CH_2IBr: (a) CH_2Br^+, (b) Br^+, (c) CH_2I^+, and (d) I^+. The surface colors denote the fractional yield as compared to the maximum recorded signal: 95% (maroon), 90% (red), 80% (orange), 60% (yellow), 40% (green), 20% (cyan), 10% (blue), and 5% (magenta). The landscapes in (a) and (c) are split along the A axis, as in Figure 1(b). The optimal regions of the landscapes (b) and (d) are located away from the TL pulse, which is evident with the full volume view.

B. Exploring optimal level sets

Control landscape theory predicts the possible existence of connected optimal level sets on quantum control landscapes upon satisfaction of Assumptions (i), (ii), and (iii). While the maxima of the R^+ landscapes in Figures 2(a) and 2(c) appear to have a localized maximum around the TL pulse, the two distinct landscape regions corresponding to an optimal yield of I^+ and Br^+ in Figures 2(b) and 2(d) have the structure of extended level sets. It is of interest to explore such optimal level sets on control landscapes in order to identify families of laser fields that produce an optimal yield of a target product, where one may select from among the family members for desirable secondary characteristics, such as minimization of a competing product. Here, we show that exploring the optimal level sets on the Br^+ landscape identifies regions that minimize the competing product CH_2Br^+, as well as reveals insight into the formation mechanisms of Br^+.

Figure 3(a) plots the two optimal level sets for formation of Br^+, where the colors on the surfaces denote the fractional yield of CH_2Br^+ (with respect to its maximum at the TL pulse being 1.0) according to the color bar to the right of the plot. The two disconnected level sets correspond to at least 95% of the maximum Br^+ yield recorded over the entire landscape (the maroon regions in Figure 2(b)). The two landscape regions in Figure 3(a) are labeled level set (I) and level set (II), with arrows denoting interesting points A through E on (I) and points F through J on (II). The color-coded level sets show that the fractional yield of CH_2Br^+ varies by a factor of ~4, from 0.08 to 0.32, over the optimal Br^+ level sets. This result demonstrates that optimal level sets may be exploited to understand and discover how to simultaneously minimize the yield of a competing fragmentation product (here, CH_2Br^+). This procedure gives valuable insight beyond the common operation of optimizing the corresponding product ratio, as in Refs. 10–18. In the present case of considering CH_2IBr, any point on the optimal level set corresponds to a yield of Br^+ that is larger by more than a factor of two compared to the Br^+ yield when the ratio objective Br^+/CH_2Br^+ is directly optimized with a GA using the polynomial control basis.[17] Optimizing the ratio objective directly with a GA produces ~50% of the Br^+ yield observed on the optimal level set, while the GA simultaneously minimized the yield of CH_2Br^+ to approximately 2% (i.e., lower than the minimum of 8% on the Br^+ level set at point F). Thus, directly optimizing the ratio objective Br^+/CH_2Br^+ with the GA produces a higher value than can be attained on the Br^+ level set. The latter result indicates that the landscape formed from the ratio of the landscape in Figure 2(b) to that in Figure 2 (a) exhibits additional features beyond those found on the individual product landscapes. Interestingly, a location on the Br^+ level set may also be found where the nominally competing bond-breaking products of Br^+ and CH_2Br^+ are *both* produced in high yields, although the restriction to the Br^+ level set surface with variables A, B, and C does not include the TL pulse producing maximum CH_2Br^+ yield. Importantly, this collective behavior shows that a complex interplay of bond breaking and ionization are at work in mass spectral detection. Exploiting landscapes and level sets may be useful to untangle this complex behavior, but the experiments typically require significant effort because the structures of the landscapes are generally not known *a priori* and must be mapped out by sampling to a desired resolution.

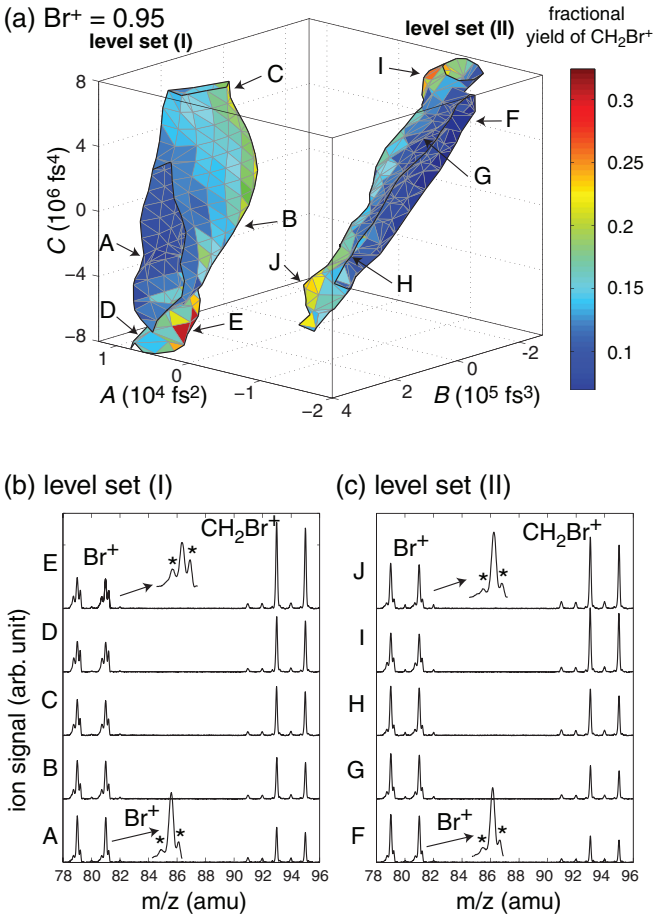

FIG. 3. (a) Optimal Br^+ level sets (I) and (II) from CH_2IBr. The fractional yield of CH_2Br^+ is indicated by the color bar. (b) TOF mass spectra showing the region containing Br^+ and CH_2Br^+ for the points A through E of level set (I). (c) TOF mass spectra showing the same region for the points F through J of level set (II). The peaks corresponding to the ^{79}Br and ^{81}Br isotopes are visible in both the Br^+ and the CH_2Br^+ signals. The magnified Br^+ signals in A, E, F, and J show the multi-peak fine structure of the ion signals, with the peaks arising from the Coulomb explosion formation mechanism indicated by an asterisk (*).

The corresponding TOF spectra of the region containing Br^+ and CH_2Br^+ are shown in Figures 3(b) for points A through E and 3(c) for points F through J, where the TPA signal increases ascending the ordinate on both plots (b) and (c), ranging from ~20% of its maximum signal (from the TL pulse) at points A and F to ~50% of its maximum signal at points E and J. The spectra show the different yields of CH_2Br^+ and also reveal the varying contributions of the Br^+ formation mechanisms across the optimal level sets. All ion signals of Br^+ contain a fine structure of three peaks, as shown by the magnified ion signals on spectra A, E, F, and J in Figures 3(b) and 3(c). The larger central peak corresponds to Br^+ formed from the dissociation of a singly charged precursor ion. The two outer peaks (labeled with an asterisk (*) on the magnified ion signals) come from the Coulomb explosion of a multiply-charged precursor ion, which produces ions with

an initial kinetic energy projected along the TOF axis towards (left peak) or away (right peak) from the detector.[59] Across level set (I), the height of the Coulomb explosion peaks exhibits significant variation, as shown by the magnified Br^+ signals at points A and E. There is a trade-off between the height of the center peak and the Coulomb explosion peaks, indicating that two distinct formation mechanisms compete across the level set, where the center peak is favored at lower-intensity pulses (with small CH_2Br^+ signals, points A and B), while the Coulomb explosion peaks are favored at higher intensity (point E). In contrast, the Br^+ ion signals on all spectra from level set (II) are dominated by the non-Coulomb explosion peak, even when the TPA signal is high (e.g., point J). These distinct features of level sets (I) and (II) suggest there may exist an underlying physical basis for the disconnectedness of the two optimal Br^+ level sets in Figure 3(a).

C. Assessing the effects of control constraints

The landscapes in Sec. III A with varying A, B, and C at maximum pulse energy were found to exhibit features consistent with the predictions of control landscape theory, particularly indicating that these experimental variables and conditions did not appear to violate Assumption (iii). Here, we consider two explicit constraints placed on these control variables. First, the number of control variables is reduced from three to two, with A and B varied, but C fixed at specific values. Second, the laser pulse energy is reduced, with A, B, and C allowed to vary over their complete ranges.

1. Constraining the number of control variables

For the Br^+ landscape in Figure 2(b), full variation of A, B, and C is necessary to produce a trap-free landscape topology. When only A and B are varied (with a fixed value of C), apparent (i.e., "false" due to the extra constraint) traps are encountered on the resulting two-dimensional control landscapes, as shown in Figure 4 for $C = -4 \times 10^6$ fs^4 (a), $C = 0$ fs^4 (b), and $C = 4 \times 10^6$ fs^4 (c), where traps are marked on all three landscapes with an "x." These traps may have contributions from apparatus aberrations, but importantly there are no apparent traps on the landscape upon allowing full variation of C, as is evident in Figure 2(b). Although three polynomial phase variables are evidently sufficient in order to satisfy Assumption (iii) of control landscape theory to a practical degree for Br^+ formation from CH_2IBr, other objectives or compounds may require additional control variables to satisfy the same assumption.

2. Constraining the pulse energy

Limiting the laser pulse energy can present a significant experimental constraint in some applications, and pulse energy is always a limited resource in the laboratory. Here, we consider the effects of constraining the laser pulse energy by limiting the transmission of the laser radiation through the SLM by means of uniform amplitude reduction over the laser bandwidth resulting in the pulse energy being reduced to 310 μJ, 280 μJ, and 250 μJ per pulse from the maximum

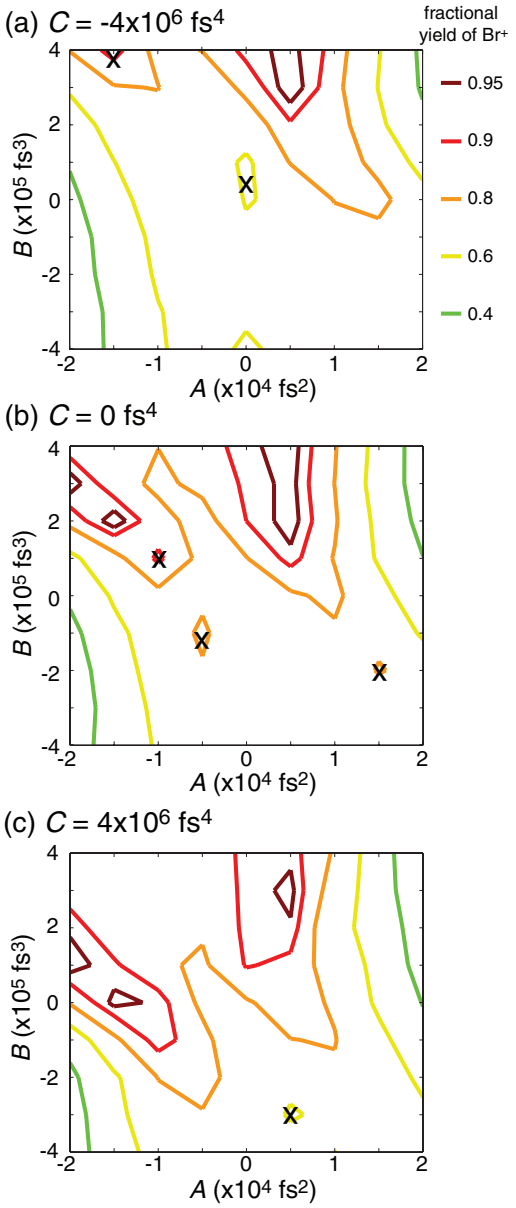

FIG. 4. Landscapes for Br^+ yield constrained to two variables A and B in Eq. (2) with C fixed at -4×10^6 fs^4 (a), 0 fs^4 (b), and 4×10^6 fs^4 (c). The contour lines correspond to the same fractional yields of Br^+ as in Figure 2(b). Traps are marked with an "x" on the landscapes. The three-dimensional landscape in Figure 2(b), however, contains no obvious traps.

available (i.e., 350 μJ per pulse). The control variables A, B, and C are allowed to vary over their full ranges, as in Sec. III A. The landscapes for the fragments CH_2I^+ and CH_2Br^+ had the same general shape as the associated landscapes in Figures 2(a) and 2(c), but with reduced yields at each landscape point (not shown). The landscapes for Br^+ are examined in detail below, and the landscapes for I^+ exhibited qualitatively similar features (not shown).

Figure 5 presents the landscapes for Br^+ yield at pulse energies of (a) 310 μJ, (b) 280 μJ, and (c) 250 μJ. The reported level set yields on the landscapes are with respect to the maximum Br^+ yield in Figure 2(b). At 310 μJ pulse energy (Figure 5(a)), the optimal level set of 95% Br^+ yield shrinks to essentially a point in the region of level set (II) in

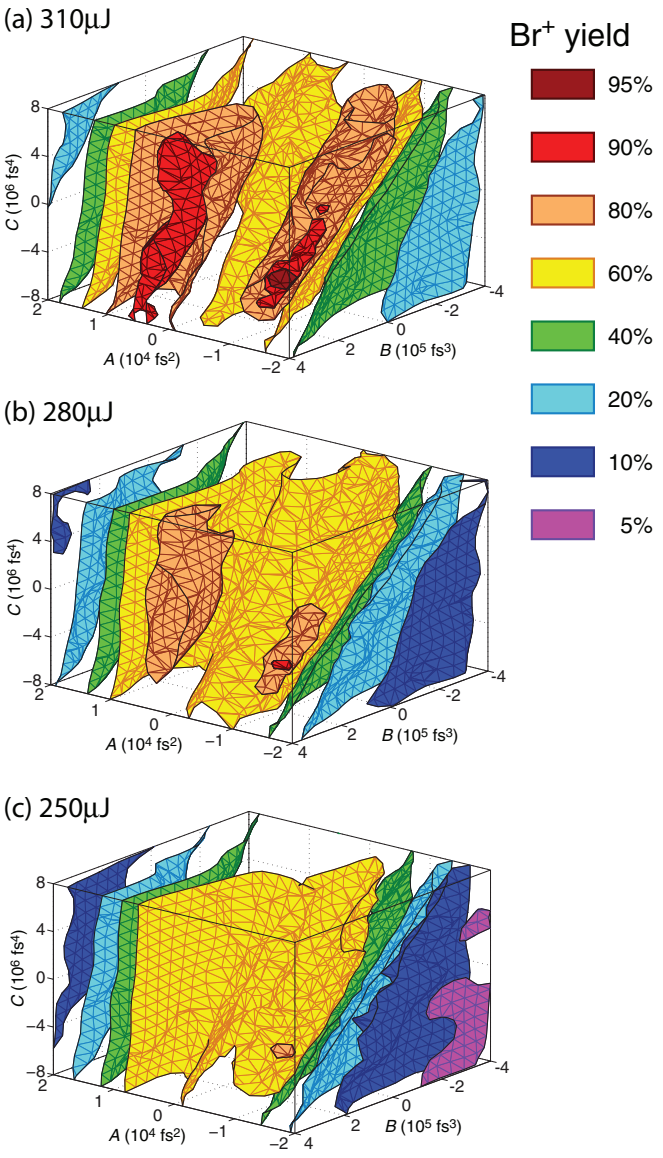

FIG. 5. Landscapes for Br^+ yield from CH_2IBr at pulse energies of 310 μJ (a), 280 μJ (b), and 250 μJ (c). All reported fractional yields are with respect to the maximum yield with full pulse energy of 350 μJ in Figure 2(b). At 310 μJ, the maximum 95% Br^+ yield is still attainable, but only at a small localized point, and a large trapping region at 90% yield arises. As the pulse energy drops further, the maximum attained yield is reduced, and traps are observed. This behavior reflects a gradual retreat of the control landscape from its inherent unconstrained form.

Figure 3(a), and level set (I) is no longer optimal, instead corresponding to a large trapping region at 90% yield. This result shows that for the creation of Br^+, even a modest decrease in the pulse energy below the 350 μJ available in our experiments produces a significant constraint that precludes satisfaction of Assumption (iii) of control landscape theory, as a trap appears on the control landscape. This behavior suggests that even greater yields of Br^+ may be obtained at higher pulse energy than the maximum of 350 μJ available in our experiments. When the pulse energy is reduced to 280 μJ (Figure 5(b)), the maximum Br^+ yield is 90% at an isolated location near the landscape point that produced 95% yield in Figure 5(a), and a large trapping region exists at 80% yield in the area corresponding to the 90% yield trap in

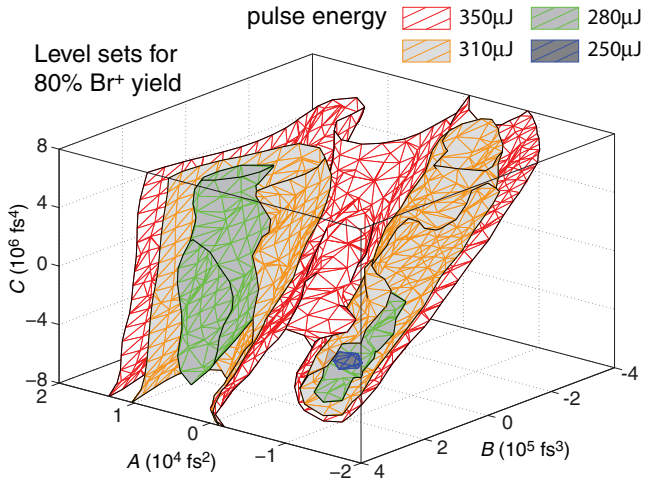

FIG. 6. Level set for 80% Br^+ yield from CH_2IBr (compared to the maximum yield at full laser pulse energy in Figure 2(b)) as a function of pulse energy. The colors of the vertices correspond to the pulse energy: red = 350 μJ, orange = 310 μJ, green = 280 μJ, blue = 250 μJ. The 80% Br^+ yield level set shrinks to an isolated point at 280 μJ pulse energy.

Figure 5(a). At 250 μJ pulse energy (Figure 5(c)), the 80% level set is reduced to an isolated point and is the highest yield on the landscape. These landscapes show that imposing constraints on the laser pulse energy below some threshold value (here, ~310 μJ, Figure 5(a)) introduces traps on the Br^+ landscape.

As another perspective on the shrinkage of landscape regions producing a good, but not optimal yield, we illustrate the level set corresponding to 80% Br^+ yield as the pulse energy is reduced. The 80% yield level set for full pulse energy, as well as at the reduced pulse energies, are plotted together in Figure 6. At full pulse energy of 350 μJ, there is one continuous level set of 80% yield (white/red). As the pulse energy is decreased to 310 μJ, the level set fractures into two disconnected regions (light grey/orange), which are analogous to level sets (I) and (II) in Figure 3. These level sets shrink at 280 μJ pulse energy (grey/green). The original level set (I) disappears completely at 250 μJ, while the original level set (II) shrinks to an isolated point (dark grey/blue). The fracturing, shrinkage, and disappearance of both optimal and sub-optimal level sets in Figures 5 and 6, respectively, upon lowering of the pulse energy is consistent with results from numerical simulations for simple model systems.[34] As a final comment, the dissociative ionization processes here are highly nonlinear in the applied field, which likely results in the observed sensitivity to pulse energy. Other control objectives and molecules might exhibit distinct behavior, including specially favorable performance under some constraints if those conditions limit competition from other product channels.

IV. LANDSCAPES FOR OTHER HALOGENATED HYDROCARBONS

This section presents control landscapes for the R^+ and X^+ dissociative ionization products from the halogenated

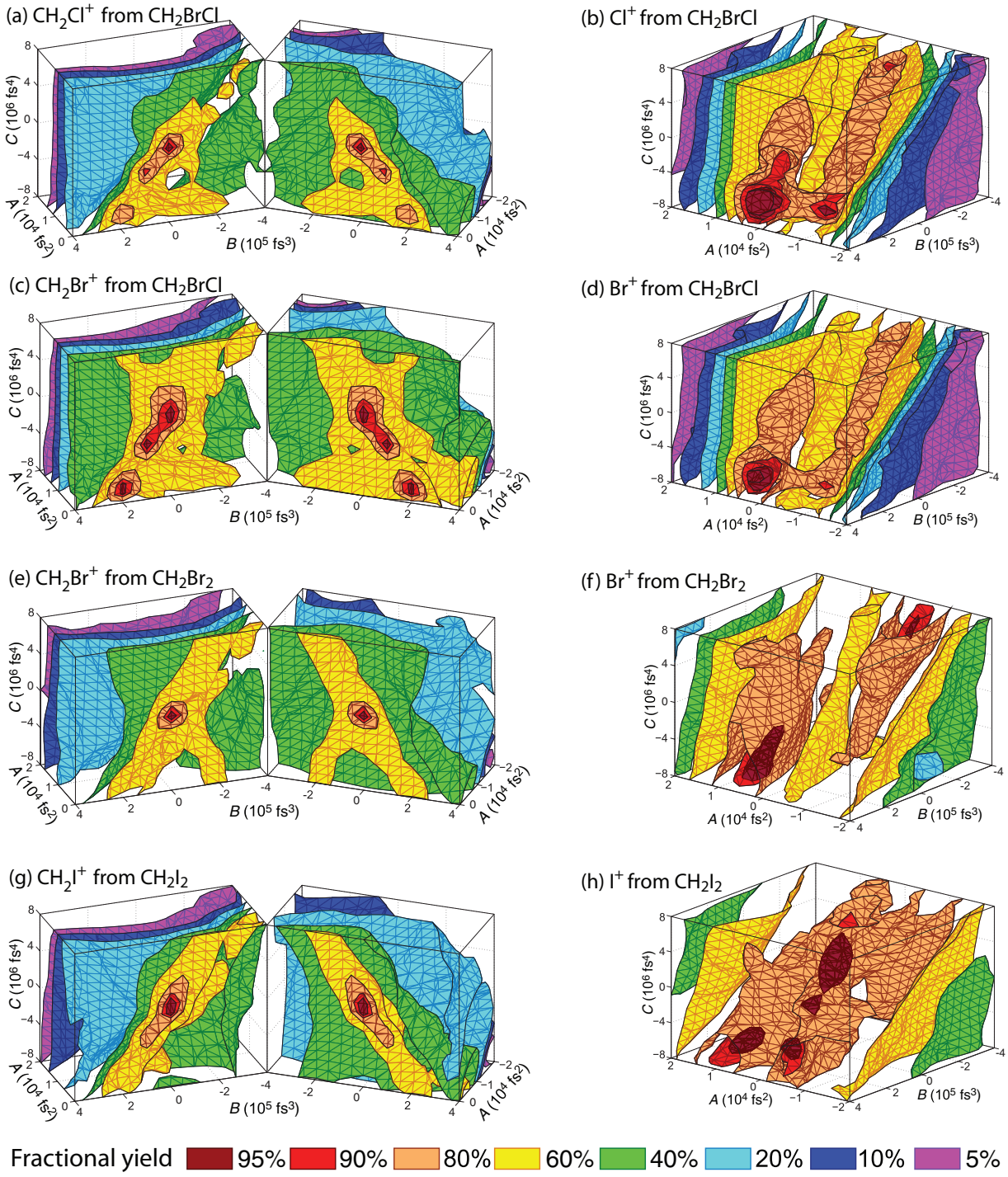

FIG. 7. Landscapes for ions from halomethanes: (a) CH_2Cl^+, (b) Cl^+, (c) CH_2Br^+, and (d) Br^+ from CH_2BrCl; (e) CH_2Br^+ and (f) Br^+ from CH_2Br_2; and (g) CH_2I^+ and (h) I^+ from CH_2I_2. All landscape maxima in (a), (c), (e), and (g) for the R^+ fragments are at the TL pulse with $A = B = C = 0$, indicating a predominant dependence on laser intensity. The landscapes for X^+ in (b), (d), (f), and (h) have different structures.

hydrocarbons CH_2BrCl, CH_2Br_2, CH_2I_2, C_3H_5Br (mixture of *cis*/*trans* 1-bromo-1-propene), C_4H_7Cl (3-chloro-2methyl-1-propene), and C_6H_5Cl (chlorobenzene). The goals are to (i) examine the landscape features across the set of related compounds and (ii) further assess the predictions of control landscape theory, as will be discussed in Secs. V and VI, respectively.

Figure 7 shows the R^+ and X^+ landscapes for the halomethanes CH_2BrCl, CH_2Br_2, and CH_2I_2. The landscapes for the R^+ species are (a) CH_2Cl^+ and (c) CH_2Br^+ from CH_2BrCl; (e) CH_2Br^+ from CH_2Br_2; and (g) CH_2I^+ from CH_2I_2. The maximum yield for these R^+ landscapes occurs at the TL pulse, as was the case for the R^+ landscapes from CH_2IBr in Figures 2(a) and 2(c). In contrast, the landscapes for the X^+ fragments (b) Cl^+ and (d) Br^+ from CH_2BrCl; (f) Br^+ from CH_2Br_2; and (h) I^+ from CH_2I_2 generally have disconnected optimal regions away from the TL pulse. The I^+ landscape for CH_2I_2 has these optimal regions

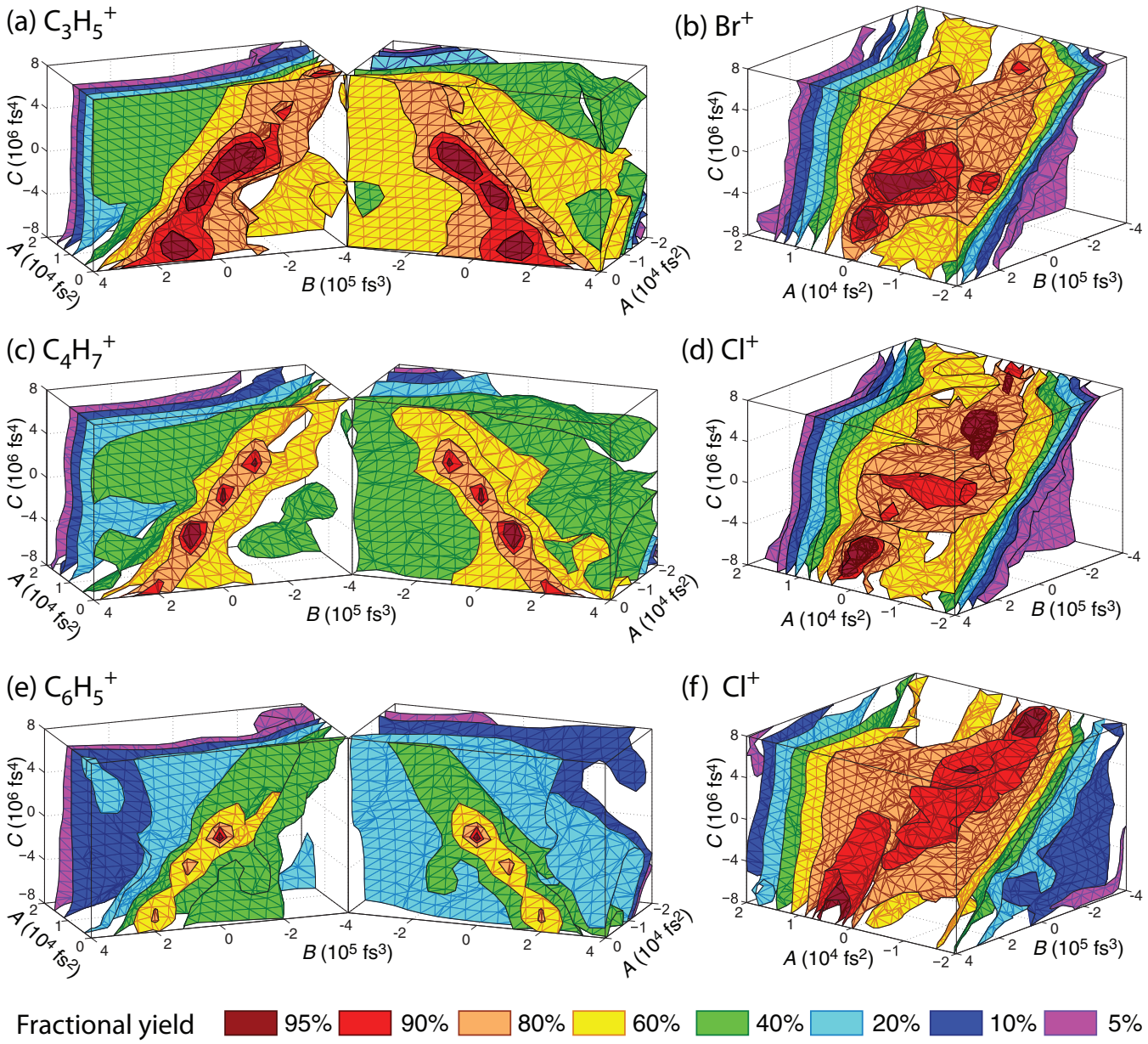

FIG. 8. Landscapes for fragments from the species C_3H_5Br, C_4H_7Cl, and C_6H_5Cl. (a) $C_3H_5^+$, (b) Br^+ from C_3H_5Br; (c) $C_4H_7^+$, (d) Cl^+ from C_4H_7Cl; and (e) $C_6H_5^+$, (f) Cl^+ from C_6H_5Cl. The landscapes in (a), (c), and (e) look similar to each other and to the landscapes in Figures 2(a) and 2(c), and Figures 7(a), 7(c), 7(e), and 7(g), indicating a predominant intensity dependence. The halogen landscapes in (b), (d), and (f) exhibit distinct structures.

including a large domain around the TL pulse. The landscapes in Figures 7(a), 7(b), and 7(d) appear to contain one or more trapping points at 80% or 90% yield. However, it is not possible to definitively characterize these regions as landscape traps, as various additional factors may be involved here including finite SLM resolution, noise in the laser pulses or signals, inadequacy of the polynomial basis, etc., which will be discussed further in Sec. VI.

Landscapes for the R^+ and X^+ products of C_3H_5Br, C_4H_7Cl, and C_6H_5Cl are shown in Figure 8: (a) $C_3H_5^+$, (b) Br^+ from C_3H_5Br; (c) $C_4H_7^+$, (d) Cl^+ from C_4H_7Cl; and (e) $C_6H_5^+$, (f) Cl^+ from C_6H_5Cl. As was the case for the halomethanes, all of the landscapes for the R^+ yield in Figure 8 are correlated with laser intensity, with the landscape maximum around the TL pulse. The landscapes for X^+ yields in Figures 8(b), 8(d), and 8(f) exhibit (i) distinct structures from the R^+ landscapes and (ii) have similar overall character to the halogen ion yields from halomethanes with multiple optima away from the TL pulse. Similar to Figure 1, the apparent traps at 80% or 90% yield in Figures 8(b)–8(e) will be discussed in Sec. VI.

V. RULES FOR PREDICTING LANDSCAPE FEATURES

The photoproducts of all of the halogenated hydrocarbons examined in this work show that the landscapes for the R^+ fragment yield share a similar predominant intensity-dependent structure, while the landscapes for the X^+ yield exhibit common features indicating the presence of a complex control process beyond the role of laser intensity.

Further experiments are currently underway in our laboratory to investigate the ionization and dissociation processes leading to preferential formation of X^+. The collective shared landscape behavior implies that the chemical homology of these halogenated hydrocarbons extends to their interaction with a related family of shaped laser pulses acting as "photonic reagents." The results may be summarized by two general landscape rules:

- **Rule I:** The maximum yield on an R^+ landscape is localized around the TL pulse, with the landscape resembling that of the intensity-dependent TPA yield.
- **Rule II:** An X^+ landscape contains two or more large areas of maximum yield away from the TL pulse, at positive and negative values of A.

These rules qualitatively characterize the landscapes for R^+ and X^+ fragments produced by photonic reagents described by the present set of control variables. In addition, the rules encompass homologous behavior found previously across a large family of halomethanes[17,50] to now include the species C_4H_7Cl, C_3H_5Br, and C_6H_5Cl, which collectively cover significant diversity in hydrocarbon composition. Codifying these rules presents a first step towards developing a systematic basis for predicting the outcomes of photonic-reagent induced reactions, in analogy to commonly utilized empirical rules for predicting the outcomes of reactions induced by chemical reagents.[51,52] Further exploration of control landscapes for other types of molecular families is needed to identify an expansive systematic foundation for photonic-reagent induced reactions.

Rules I and II explain previous optimal control results for selective fragmentation of halomethanes.[12,13,17,50] Based on Rule I, in halomethanes containing two different types of halogen atoms, only limited enhancement can be achieved for the objective of breaking the stronger carbon-halogen bond while leaving the weaker carbon-halogen bond intact, as reflected in the ratio of the respective R^+ yields. For example, in CH_2BrCl, the enhancement of the ratio CH_2Br^+/CH_2Cl^+ by only a factor of ~2–3 over the TL pulse was achieved.[12,17] In CH_2IBr, the analogous ratio CH_2I^+/CH_2Br^+ could only be enhanced by a factor of ~2–2.5.[13,17] The landscapes in the present work show that the latter results can be attributed to both R^+ fragments obeying Rule I and having very similar landscapes (i.e., compare Figures 2(a) and 2(c) for CH_2IBr and Figures 7(a) and 7(c) for CH_2BrCl). In contrast, recent work[17,50] indicates that significantly greater control can be achieved over the product ratios of X^+/R^+, with control enhancements typically exceeding a factor of ~25 for CH_2BrCl, CH_2Br_2, CH_2IBr, and CH_2I_2 as compared to the TL pulse. This wide dynamic range of control can be understood from the X^+ fragments obeying Rule II and the R^+ fragments obeying Rule I; the broad maximum level sets for the X^+ fragment permits identifying photonic reagents that also minimize the R^+ signal. These collective results also show that conclusions about the ability to break a strong versus weak bond is linked to the choice of ionized product species for comparison when using mass spectrometric detection. Importantly, the actual selective control is over the combined dissociation and ionization of the species. Measurement of the neutral product fragments and their landscapes is needed for a full picture of bond-breaking selectivity. Notwithstanding these issues, the present results show that identifying rules governing the formation of specific fragmentation products based on their landscapes can aid in explaining controlled branching ratios. The competitive nature of the rules for some fragments can also be viewed as arising from a Pareto optimization[60] utilizing pairs of individual product landscapes. The discovery of analogous rules for other classes of molecules should provide insight into the dynamic ranges of the yields for selective fragmentation objectives.

VI. ASSESSMENT OF CONTROL LANDSCAPE THEORY PREDICTIONS

Defining the "unconstrained" control variables as A, B, and C along with a pulse energy of 350 μJ leads to landscapes from CH_2Br_2, CH_2IBr, and CH_2I_2 without trapping extrema, although additional control resources may produce yet higher yields and more expansive landscapes. The results indicate that the corresponding experimental control objectives satisfy the three Assumptions of control landscape theory.[21–24] While Assumptions (i) and (ii) may often be taken for granted, as discussed in the Introduction,[25–27] the satisfaction of Assumption (iii) is difficult to assess *a priori*. Thus, many of the landscapes revealed in this work indicate that the operational limitations in the laser pulse energy, spectral bandwidth, and/or the number of independent polynomial phase control variables were not significant enough to destroy the underlying control landscape topology predicted from adequate satisfaction of all three Assumptions. However, some landscapes for CH_2BrCl, C_3H_5Br, C_4H_7Cl, and C_6H_5Cl appear to contain traps, albeit at a high yield of $\gtrsim$80% of the observed maximum, when operating with all available control variables. In these cases, the likely conclusion is that Assumption (iii) was violated due to one or more of the following experimental constraints and circumstances:

(A) The available laser pulse energy may be inadequate for full control of fragmentation.
(B) The center wavelength, spectral bandwidth, etc., of the laser pulses may be inadequate.
(C) The number and/or type of control variables may be inadequate. As the total number and type of control variables needed to reveal the full underlying control landscapes is unknown, more variables may be necessary to remove traps on some landscapes.
(D) The finite resolution of the SLM and possible contributions from optical alignment issues may artificially distort the landscape, such that the constructed pulses do not reliably reflect the polynomial phase variables. A similar problem distorted a landscape reported in Ref. 41.
(E) Noise in the pulse energy and/or spectral phase may cause subtle variations in the recorded ion signals that produce apparent traps. Even with extensive signal averaging, the estimated error in the recorded ion yields is ~±5%.

None of the above constraints or limitations can be completely eliminated in practice, and it is natural to seek the minimal resources or variables in (A), (B), and (C) that meet the goal of finding trap-free landscapes.

The apparent trapping regions at 90% yield on the X^+ landscapes in Figures 7(b), 7(d), 8(b), and 8(d) may be analogous to those on the landscapes in Figure 5 upon reduction of the pulse energy, which suggests that constraint (A) may play a role. For CH_2BrCl, it is reasonable to assume that insufficient laser pulse energy contributes to the observed traps on the landscapes in Figures 7(b) and 7(d) because the appearance energies of Br^+ and Cl^+ from CH_2BrCl are significantly higher than for CH_2Br_2, CH_2IBr, and CH_2I_2,[50] which have trap-free landscapes with full pulse energy of 350 μJ. Thus, we speculate that if a higher pulse energy were available, the traps on the landscapes for CH_2BrCl could be lifted. Constraint (A) may also contribute to the observed traps for X^+ yield from C_4H_7Cl and C_3H_5Br as well, but this consideration cannot be evaluated without knowing the appearance energies of the halogen ions from C_3H_5Br and C_4H_7Cl, which are not reported in the literature to our knowledge. Constraint (D) may also play a role in producing the high yield traps observed on the landscapes in Figures 2(a), 7(a), 8(c), and 8(e) because these traps are located in the region with $C < 0$ corresponding to a similar unusual structure on the TPA landscape in Figure 1. Finally, any of the traps may be caused by constraints (B), (C), and (E), respectively, because the contributions of the center wavelength and spectral bandwidth are unknown, the number and type of control variables needed to reveal the full underlying landscape is not known for any of these compounds, and noise in the laser pulses can never be eliminated.

These common experimental limitations suggest that at least some of the observed traps may be lifted with additional resources in (A), (B), and (C). Furthermore, many of the reported traps occur at 90% yield relative to the observed maximum, implying that the traps are near the global landscape optima. Numerical simulations with model systems indicate that imposing constraints initially shows up on the landscape by producing traps only at regions corresponding to a high yield, while even stronger constraints produce much more detrimental traps at still lower yields.[34] Thus, the traps on the present experimental landscapes appear to fall into a mild constraint regime, so we expect that a modest expansion of experimental resources may lift many of the traps on the landscapes.

A major control landscape theory prediction is that the optimal landscape regions can have the structure of connected level sets.[22,23] Most of the X^+ landscapes in this work had this feature. Control landscape theory also permits the existence of multiple disconnected optimal level sets,[33] as was found in the majority of the X^+ landscapes. Furthermore, multiple disconnected optimal level sets were observed in simulations when small numbers of control variables were used,[34] which is also consistent with the present results. The two apparently distinct optimal level sets on the X^+ landscapes observed here may actually be connected upon using a larger number of control variables or with extended ranges of the current variables, but these situations cannot be assessed within the experimental limitations of this work. However, what appear to be distinct control mechanisms separately operating on the two disconnected optimal level sets in Figure 3 suggest that there is a physical basis for their being disconnected.

Molecular dynamics phenomena, especially dissociation, are described in an extremely high, even infinite dimensional Hilbert space. This situation would seem to imply that it would be difficult to satisfy the three Assumptions of control landscape theory, especially (iii).[22] However, many of the control objectives considered in this work appear to satisfy the landscape theoretical predictions, while only working with three reasonably chosen control variables. This conundrum suggests that the dynamics of the control processes here may have a far reduced *effective dynamic dimension* (EDD)[61] compared to the molecule's Hilbert space. Control landscape theory predicts a quantitative relation between the dimension of the control system and the dimensionality of the optimal level sets on the control landscape.[22,61] In particular, for an N-dimensional quantum system at the landscape optimum under state-to-state control, there are at most $2N - 2$ independent directions (i.e., control variables) that lead off of the optimum to decrease the yield. In this situation, when K independent control variables are employed, the dimensionality of the optimal level set (i.e., the number of control variables that describe the optimal level set) is at least $K - 2N + 2$. For more general observable control (i.e., of the form in Eq. (1)), the number of directions that lead off the top of the landscape is bounded from above by N^2.[24] The $2N - 2$ prediction for state-to-state control has been verified in numerical simulations,[31,33,34] as well as in an experiment on atomic rubidium.[62] The present results on dissociative ionization highlight the value of performing more thorough landscape analyses, including with more variables, to establish the EDD and the associated important variables at the top of the landscape.

VII. CONCLUSION

Experimental optimization of any control objective involves a search over the underlying control landscape. Control landscape theory predicts that no sub-optimal traps should exist upon the satisfaction of the Assumptions that (i) the objective is controllable, (ii) freedom exists to move locally over the landscape around the final state, and (iii) no significant constraints are placed on the control variables. The resultant favorable landscape topology was put forth as a basis to explain the widely reported efficient and generally successful optimization of many experimental control objectives.[19,21] This work employed a physically reasonable set of three control variables that additionally permitted visual exploration of experimental control landscapes. The visualization of the landscapes enabled assessment of landscape theory for the yields of ionized fragmentation products from the dissociation of halogenated hydrocarbons. In this regard, the use of only a small number of independent polynomial phase control variables is expected to constitute a stringent test of control landscape theory.

The results in this work showed that many of the control landscapes for the yields of ionized molecular fragmentation products exhibit a trap-free topology, indicating

satisfaction of the underlying Assumptions to a practical degree, despite the experimental limitations. While experimental trap-free control landscapes with two or three control variables have been observed for a variety of nonlinear optical processes,[38,40–45] this work constitutes the first experimental validation of control landscape theory for objectives defined by the yield of photochemical fragmentation reaction products. Importantly, it is essential to properly choose a physically suitable set of control variables, especially when operating with few of them.[34] The ability to control the yield of chemical reactions with only a small number of suitable independent variables is widely observed in the optimization of chemical reactions without lasers, which share the same control landscape topology.[51,52] The current results for controlling chemical reactions with tailored laser pulses acting as photonic reagents thus complement the observed control of chemical reactions with traditional chemical reagents.

The observation of favorable trap-free landscapes despite extensive experimental limitations may be due to the presence of an underlying simple control process reflected in terms of an operational EDD, as discussed in Sec. VI. Once again, when employing only a few variables, their proper choice is essential. For example, operating with a pulse shaper pixel basis produces a large number of variables, but a representation in a mathematically equivalent but physically more suitable basis may aid the optimization process. Further investigation[62] is needed to fully assess the presence of an EDD of the controlled dissociative ionization processes, which may explain the satisfaction of control landscape theory predictions even with modest resources.

The presence of traps on some of the control landscapes in this work indicates that more freedom in the experimental resources, e.g., a greater pulse energy and/or a greater number of various types of independent phase variables, may be needed in order to more broadly satisfy the Assumptions of control landscape theory. Thus, the development of methods to systematically explore experimental control landscapes in higher dimensions is crucial to further the understanding of laboratory optimal quantum control. Such multi-dimensional experimental methods would also enable investigation of control landscapes for more complex chemical processes than those examined here.

The presence of two optimal level sets on some landscapes for some X^+ species also provides further insight into dissociative ionization. The control mechanism for Br^+ formation from CH_2IBr in terms of its origins from a singly or multiply charged precursor was also found to vary across the level sets. Distinct control mechanisms have been observed on level sets for nonlinear optical processes as well.[38] Exploration of the optimal level sets for Br^+ yield also enabled identification of a laser pulse that simultaneously minimized the yield of the competing fragment CH_2Br^+, while maintaining a high Br^+ yield. This result shows that exploration of optimal level sets, along with access to multiple product landscapes can permit effective Pareto optimization of the yields of competing products. Similar methods could be used to identify points on optimal level sets that have some other beneficial property, such as being especially robust to noise.[33]

The common rules across the chemical family of halogenated hydrocarbons discussed in Sec. V link the photonic reagent landscape analysis in this work with like chemical reagent landscape analyses, expressed by OptiChem theory.[51,52] The common behavior across the halogenated hydrocarbon bolsters earlier observed systematic trends in dissociative ionization reactions over a family of halomethanes,[17,18,50] thereby further connecting the two optimization domains with photonic and chemical reagents. In particular, the common features of the landscapes, respectively, for the R^+ and X^+ species, across a chemically related family of molecules presents a first step towards deducing predictive rules for photonic reagent chemistry in analogy to those often used to guide investigations in traditional chemistry.

The exploration of experimental control landscapes is of fundamental interest and of practical importance for identifying particularly favorable control solutions. The results in this paper reveal only a glimpse of landscape features for experimental molecular fragmentation objectives, and control landscapes for the fragmentation products of other families of molecules need to be explored to generalize the present findings.

ACKNOWLEDGMENTS

The authors acknowledge support from NSF Grant No. CHE-1058644, DOE Grant No. DE-FG02-02ER15344, and ARO Grant No. W911NF-13-1-0237.

[1]R. Judson and H. Rabitz, Phys. Rev. Lett. **68**, 1500 (1992).
[2]H. Wen, C. Rangan, and P. Bucksbaum, Phys. Rev. A **68**, 053405 (2003).
[3]T. Brixner, N. H. Damrauer, B. Kiefer, and G. Gerber, J. Chem. Phys. **118**, 3692 (2003).
[4]R. Bartels, S. Backus, E. Zeek, L. Misoguti, G. Vdovin, I. P. Christov, M. M. Murnane, and H. C. Kapteyn, Nature (London) **406**, 164 (2000).
[5]R. Bartels, M. Murnane, H. Kapteyn, L. Christov, and H. Rabitz, Phys. Rev. A **70**, 043404 (2004).
[6]T. Pfeifer, R. Kemmer, R. Spitzenfeil, D. Walter, C. Winterfeldt, G. Gerber, and C. Spielmann, Opt. Lett. **30**, 1497 (2005).
[7]J. L. Herek, W. Wohlleben, R. J. Cogdell, D. Zeidler, and M. Motzkus, Nature (London) **417**, 533 (2002).
[8]G. Vogt, G. Krampert, P. Niklaus, P. Neurnberger, and G. Gerber, Phys. Rev. Lett. **94**, 068305 (2005).
[9]V. I. Prokhorenko, A. M. Nagy, S. A. Waschuk, L. S. Brown, R. R. Birge, and R. J. D. Miller, Science **313**, 1257 (2006).
[10]A. Assion, T. Baumert, M. Bergt, T. Brixner, B. Kiefer, V. Seyfried, M. Strehle, and G. Gerber, Science **282**, 919 (1998).
[11]R. Levis, G. Menkir, and H. Rabitz, Science **292**, 709 (2001).
[12]N. Damrauer, C. Dietl, G. Krampert, S. Lee, K. Jung, and G. Gerber, Eur. Phys. J. D **20**, 71 (2002).
[13]D. Cardoza, C. Trallero-Herrero, F. Langhojer, H. Rabitz, and T. Weinacht, J. Chem. Phys. **122**, 124306 (2005).
[14]F. Langhojer, D. Cardoza, M. Baertschy, and T. Weinacht, J. Chem. Phys. **122**, 014102 (2005).
[15]D. Cardoza, M. Baertschy, and T. Weinacht, Chem. Phys. Lett. **411**, 311 (2005).
[16]D. Cardoza, M. Baertschy, and T. Weinacht, J. Chem. Phys. **123**, 074315 (2005).
[17]K. Moore Tibbetts, X. Xing, and H. Rabitz, "Optimal control of molecular fragmentation with homologous families of photonic reagents and chemical substrates," Phys. Chem. Chem. Phys. (published online).
[18]K. Moore Tibbetts, X. Xing, and H. Rabitz, "Laboratory transferability of optimally shaped laser pulses for quantum control," J. Chem. Phys. (submitted).
[19]C. Brif, R. Chakrabarti, and H. Rabitz, New J. Phys. **12**, 075008 (2010).

[20]W. Zhu, J. Botina, and H. Rabitz, J. Chem. Phys. **108**, 1953 (1998).
[21]H. Rabitz, M. Hsieh, and C. Rosenthal, Science **303**, 1998 (2004).
[22]H. Rabitz, T.-S. Ho, M. Hsieh, R. Kosut, and M. Demiralp, Phys. Rev. A **74**, 012721 (2006).
[23]R. Wu, M. Hsieh, C. Rosenthal, and H. Rabitz, J. Phys. A: Math. Theor. **41**, 015006 (2008).
[24]H. Rabitz, M. Hsieh, and C. Rosenthal, J. Chem. Phys. **124**, 204107 (2006).
[25]V. Ramakrishna, M. V. Salapaka, M. Dahleh, H. Rabitz, and A. Pierce, Phys. Rev. A **51**, 960 (1995).
[26]R. Chakrabarti and H. Rabitz, Int. Rev. Phys. Chem. **26**, 671 (2007).
[27]R. Wu, J. Dominy, T.-S. Ho, and H. Rabitz, Phys. Rev. A **86**, 013405 (2012).
[28]C. Altafini, J. Math. Phys. **43**, 2051 (2002).
[29]A. N. Pechen, and D. J. Tannor, Phys. Rev. Lett. **106**, 120402 (2011); H. Rabitz, T.-S. Ho, R. Long, R. Wu, and C. Brif, *ibid.* **108**, 198901 (2012); A. N. Pechen, and D. J. Tannor, *ibid.* **108**, 198902 (2012).
[30]K. Moore, M. Hsieh, and H. Rabitz, J. Chem. Phys. **128**, 154117 (2008).
[31]K. W. Moore and H. Rabitz, Phys. Rev. A **84**, 012109 (2011).
[32]K. W. Moore, R. Chakrabarti, G. Riviello, and H. Rabitz, Phys. Rev. A **83**, 012326 (2011).
[33]V. Beltrani, J. Dominy, T.-S. Ho, and H. Rabitz, J. Chem. Phys. **134**, 194106 (2011).
[34]K. W. Moore and H. Rabitz, J. Chem. Phys. **137**, 134113 (2012).
[35]K. W. Moore Tibbetts, C. Brif, M. Grace, A. Donovan, D. Hocker, T.-S. Ho, R. Wu, and H. Rabitz, Phys. Rev. A **86**, 062309 (2012).
[36]A. Donovan, V. Beltrani, and H. Rabitz, Chem. Phys. **425**, 46–54 (2013).
[37]A. Rothman, T.-S. Ho, and H. Rabitz, Phys. Rev. A **73**, 053401 (2006).
[38]J. Roslund, M. Roth, and H. Rabitz, Phys. Rev. A **74**, 043414 (2006).
[39]M. A. Montgomery, R. R. Meglan, and N. H. Damrauer, J. Phys. Chem. A **111**, 5126–5129 (2007).
[40]J. Roslund and H. Rabitz, Phys. Rev. A **80**, 013408 (2009).
[41]G. Vogt, P. Nuernberger, R. Selle, F. Dimler, T. Brixner, and G. Gerber, Phys. Rev. A **74**, 033413 (2006).
[42]N. Form, B. Whitaker, and C. Meier, J. Phys. B **41**, 074011 (2008).
[43]J. Schneider, M. Wollenaupt, A. Winzenburg, T. Bayer, J. Köhler, R. Faust, and T. Baumert, Phys. Chem. Chem. Phys. **13**, 8733–8746 (2011).
[44]S. Ruetzel, C. Stolzenberger, S. Fechner, F. Dimler, T. Brixner, and D. J. Tannor, J. Chem. Phys. **133**, 164510 (2010).
[45]P. Marquetand, P. Nuernberger, G. Vogt, T. Brixner, and V. Engel, EPL **80**, 53001 (2007).
[46]P. van der Walle, H. Offerhaus, J. Herek, and A. Jarafpour, Opt. Express **18**, 973 (2010).
[47]A. van Rhijn, H. L. Offerhaus, P. van der Walle, J. Herek, and A. Jarafpour, Opt. Express **18**, 2695 (2010).
[48]M. Wollenhaupt, A. Präkelt, C. Sarpe-Tudoran, D. Liese, and T. Baumert, J. Mod. Opt. **52**, 2187 (2005).
[49]T. Bayer, M. Wollenhaupt, and T. Baumert, J. Phys. B **41**, 074007 (2008).
[50]K. Moore Tibbetts, X. Xing, and H. Rabitz, J. Phys. Chem. A **117**, 8205–8215 (2013).
[51]K. W. Moore, A. Pechen, X.-J. Feng, J. Dominy, V. Beltrani, and H. Rabitz, Chem. Sci. **2**, 417 (2011).
[52]K. W. Moore, A. Pechen, X.-J. Feng, J. Dominy, V. Beltrani, and H. Rabitz, Phys. Chem. Chem. Phys. **13**, 10048 (2011).
[53]B. Sussman, R. Lausten, and A. Stolow, Phys. Rev. A **77**, 043416 (2008).
[54]M. Coughlan, M. Plewicki, and R. Levis, Opt. Express **18**, 23973 (2010).
[55]MathWorks, MATLAB, The MathWorks, Natick, MA, 1994.
[56]V. V. Yakovlev, C. J. Bardeen, J. Che, J. Cao, and K. R. Wilson, J. Chem. Phys. **108**, 2309–2313 (1998).
[57]D. Irimia and M. H. M. Janssen, J. Chem. Phys. **132**, 234302 (2010).
[58]T. Goswami, S. K. K. Kumar, A. Dutta, and D. Goswami, Chem. Phys. **360**, 47–52 (2009).
[59]J. Nibarger, S. Menon, and G. Gibson, Phys. Rev. A **63**, 053406 (2001).
[60]R. Chakrabarti, R. B. Wu, and H. Rabitz, Phys. Rev. A **78**, 033414 (2008).
[61]M. Hsieh, T.-S. Ho, and H. Rabitz, Chem. Phys. **352**, 77 (2008).
[62]J. Roslund and H. Rabitz, "Assessment of quantum control landscape principles through experimental Hessian determination," Phys. Rev. Lett. (submitted).